DOI 10.1007/s11595-016-1358-z

Fabrication and Photocatalytic Activity of Ag_3PO_4-TiO_2 Heterostructural Nanotube Arrays

MO Yanping, CHEN Feng*, YANG Yunyun, SONG Jia, XU Qiong, XU Ying*

(Department of Chemistry, School of Chemistry, Chemical Engineering & Life Sciences, Wuhan University of Technology, Wuhan 430070, China)

Abstract: To extend the absorption capability of TiO_2 into visible light region and inhibit the recombination of photogenerated electrons and holes, we put forward an effective strategy of the coupling of TiO_2 with a suitable semiconductor that possesses a narrow band gap. Meanwhile, Ag_3PO_4-TiO_2 heterostructural nanotube arrays were prepared by the two-step anodic oxidation to obtain the TiO_2 nanotube arrays and then by a deposition-precipitation method to load Ag_3PO_4. The samples were characterized by field emission scanning electron microscopy (FESEM), energy dispersive spectrometry (EDS), X-ray diffraction (XRD), and UV-vis diffuse reflectance spectroscopy (UV-vis DRS). The experimental results showed that Ag_3PO_4 nanoparticles were uniformly dispersed on the highly ordered TiO_2 nanotube arrays, which increased the visible-light absorption of TiO_2 photocatalyst. The photocurrent density and photocatalytic degradation of methyl orange indicated that the performance of Ag_3PO_4-TiO_2 heterostructural nanotube arrays was better than that of the TiO_2 nanotube arrays, which could be attributed to the effective electron-hole separation and the improved utilization of visible light.

Key words: Ag_3PO_4-TiO_2 nanotube arrays; anodic oxidation; heterostructure; photocatalysis

1 Introduction

TiO_2 is widely used due to its nontoxicity, cheap availability, chemical stability and high photocatalytic activity[1-3]. TiO_2 nanotube arrays (TiO_2 NTs) have attracted much attention for their easy recycling, large specific surface area, strong adsorption ability and enough active sites for photocatalytic reactions[4,5]. Moreover, highly ordered TiO_2 nanotube arrays have advantages of controllable structures[6], efficient electron transport channels, as well as unique hollow tube structures in favor of the functionalized modifications of materials, which can improve electromagnetism, photocatalysis, photoelectricity and antibacterial properties of TiO_2. Therefore, TiO_2 NTs have potential applications in the photoelectric conversion, photochromic materials and photocatalytic degradation of pollutants[7-11]. However, because of its large band gap (3.2 eV for anatase and 3.0 for rutile), TiO_2 can only absorb ultraviolet light (λ< 400 nm), which is about 4% of the total energy in the solar spectrum. In addition, the low efficiency of electron-hole separation restrains the practical applications of TiO_2 NTs in photoelectrochemical and photocatalytic processes[12-15]. To overcome these problems, numerous modified approaches have been developed. One promising way is to combine TiO_2 NTs with a narrower band-gap semiconductor such as CdS, BiOI and Ag_3PO_4, assisting the charge separation and improving visible-light photocatalytic activity. Ag_3PO_4 with a band gap of 2.5 eV is regarded as an appropriate candidate to construct the heterostructure with TiO_2[16,17]. Ye's research group reported the use of Ag_3PO_4 semiconductor as an active visible-light driven photocatalyst[18]. However, Ag_3PO_4 is subjected to stability issues because it is prone to photoreduction and decomposition. Yu and his coworkers modified Ag_3PO_4 photocatalyst by Ag nanoparticles and Fe(III) cocatalyst, which showed an obviously higher photocatalytic activity for the degradation of methylene orange (MO) than pure Ag_3PO_4[19]. To enhance the photocatalytic stability, the synthesis of a nanosized Ag_3PO_4 particle based photocatalyst with a higher

(Received: Jan. 5, 2015; Accepted: Mar. 4, 2015)

MO Yanping(貊艳平): E-mail: mypqyf@126.com

*Corresponding authors: CHEN Feng (陈峰): Assoc. Prof.; Ph D; E-mail: fchen@whut.edu.cn; XU Ying(徐瑛): Prof.; E-mail: xuy6289@whut.edu.cn

Funded by the Natural Science Foundation of Hubei Province (2012FFB05105)

surface area is important. Thus, by combining TiO_2 NTs with Ag_3PO_4 nanoparticles to form a heterostructure, it can be expected to improve the utilization of visible light and charge transfer efficiency of photo-generated carriers. In this work, highly ordered TiO_2 NTs decorated with Ag_3PO_4 nanoparticles were prepared by the two-step anodic oxidation of TiO_2 NTs, followed by an impregnation-precipitation method. The photocatalytic activity of the Ag_3PO_4/TiO_2 NT heterostructure was evaluated by degrading MO in aqueous solution.

2 Experimental

2.1 Materials

Titanium sheets (40 mm × 10 mm × 0.2 mm, 99.6%) were purchased from Baoji Queen Titanium Co., Ltd. Other chemicals were of analytical grade supplied by Shanghai Chemical Reagent Ltd. (China) and used as received. Distilled water was used in all experiments.

2.2 Preparation of TiO_2 nanotube arrays

The highly ordered TiO_2 nanotube arrays were fabricated via electrochemically anodic oxidation[5]. Briefly, the titanium foils were polished with a piece of sandpaper, degreased and rinsed by sonication in acetone, ethanol and deionized water. Then, the cleaned titanium foils were firstly anodized in an ethylene glycol solution containing 0.5wt% NH_4F and 2vol% H_2O using a two-electrode electrochemical cell (Ti foil as the anode and Pt foil as the cathode) at 50 V for 2 h at room temperature. After the first-step anodization, th as-obtained TiO_2 nanotube arrays were removed from Ti foil by ultrasonication in enthanol for 5 min. A second anodization was additionally performed under the same condition for 90 min to generate highly ordered TiO_2 nanotube arrays. Subsequently, the two-step anodized TiO_2 nanotube arrays were washed with distilled water, followed by annealing at 450 ℃ for 2 h in ambient air to induce anatase crystallization.

2.3 Preparation of Ag_3PO_4/TiO_2 nanotube arrays

The *p*-type Ag_3PO_4 nanoparticles were loaded onto the crystallized TiO_2 nanotubes by a deposition-precipitation method. First TiO_2 NTs were immensed in an aqueous solution containing Na_2HPO_4 and kept in there for 30 min. It was then transferred to a beaker containing 0.03 M $AgNO_3$ and kept for 30 min. Finally, the sample was rinsed with DI water. This procedure was prepared for a number of times to obtain Ag_3PO_4-TiO_2 nanotube array heterojunction (Ag_3PO_4-TiO_2 NTs), as shown in Fig.1. Hereafter AT1, AT2, and AT3 denote the samples impregnated in 0.05 M, 0.25 M, and 0.50 M Na_2HPO_4 solution, respectively.

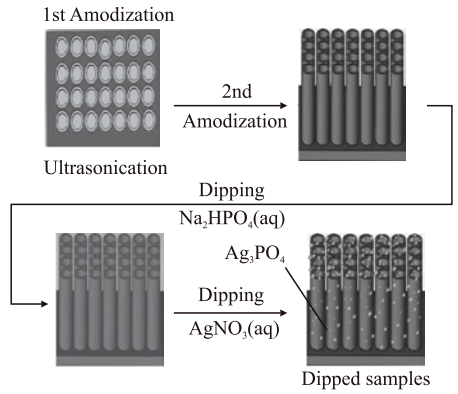

Fig.1 Schematic illustration of the preparation of Ag_3PO_4-TiO_2 heterostructural nanotube arrays

2.4 Characterization

The morphology was observed using an S-4800 field emission scanning electron microscope (FESEM, Hitachi, Japan) with energy-dispersive X-ray (EDS) analysis. Diffraction data were collected on a Rigaku Japanese company D/Max-RB diffractometer with Cu Kα radiation (40 kV×80 mA) at a scanning speed (2θ) of 3°/min. UV-vis absorption spectra of the samples were recorded on a UV-visible spectrophotometer (UV-2550, Shimadzu, Japan). $BaSO_4$ was used as a reflectance standard in a UV-vis diffuse reflectance experiment. Photoelectrochemical measurements were performed using a CHI660D (Shanghai Chenhua Equipment, China) electrochemical workstation with a three electrode system. The Ag_3PO_4-TiO_2 NT electrode was employed as the working electrode. Meanwhile, a platinum electrode and saturated calomel electrodes served as the counter and reference electrodes, respectively.

2.5 Photocatalytic activity

The photocatalytic activity of the prepared samples was evaluated via the photodegradation of methyl orange solution (MO) at ambient temperature. Experimental details were as follows: two pieces of the sample were dispersed into 20 mL of MO solution (10 mg/L) in a disk with a diameter of *ca*. 5 cm. The solution was allowed to reach an adsorption-desorption equilibrium among the photocatalyst, MO and water before irradiation. A 350W xenon lamp was used as a light source to provide simulated solar light irradiation. The average light intensity striking on the liquid surface of the reaction solution was about 40 mW/cm^2. At certain time intervals, the reaction solution was centrifuged to measure the concentration of MO determined by a UV-visible spectrophotometer (UV-

1240, SHIMADZU, Japan). As for the MO aqueous solution with low concentration, its photocatalytic decolorization is a pseudo-first-order reaction and its kinetics may be expressed as $\ln(c/c_0) = -kt$, where k is the apparent rate constant, and c_0 and c are the dye concentrations at the initial state and after irradiation for t min, respectively.

3 Results and discussion

The FESEM images of as-prepared samples are shown in Fig.2. From the top and side views of the TiO_2 NTs (Figs.2(a)-2(b)), we can see that the nanotubes are vertically aligned on the Ti substrate by the two-step anodic oxidation, with a diameter of approximately 100 nm, a wall thickness of about 40 nm and a length of about 4 nm. As can be seen from the FESEM images (Figs.2(c)-2(e)) of Ag_3PO_4-TiO_2 NTs (AT1, AT2, and AT3) by impregnation-precipitation method, uniformly dispersed Ag_3PO_4 nanoparticles, with diameter ranging from 10 to 40 nm, are successfully grown in the vertically oriented TiO_2 nanotube arrays. The presence of Ag_3PO_4 nanoparticles does not destroy the morphology of TiO_2 NTs. Most of the Ag_3PO_4 nanoparticles are evenly distributed on the top of TiO_2 NTs, while others are dispersed onto the inner wall of the nanotubes. It is apparent that the number of Ag_3PO_4 nanoparticles increases with increasing concentration of Na_2HPO_4. At the same time, the size of loaded Ag_3PO_4 nanoparticles also gradually increases. The

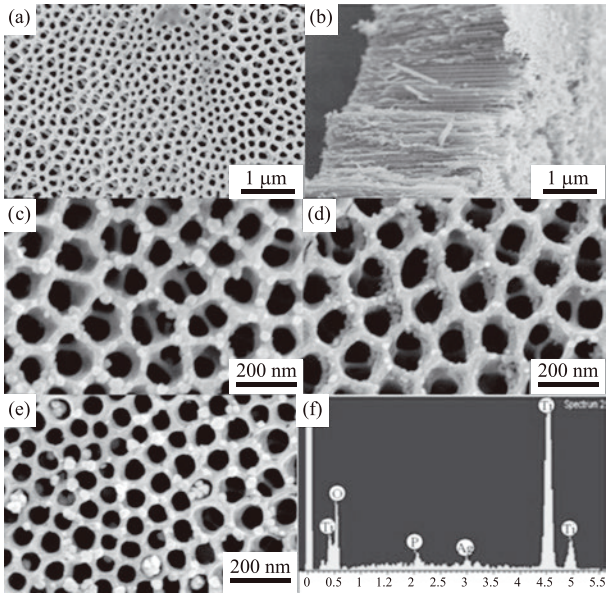

Fig.2 FESEM images and EDS spectrum of various samples: (a) top view of TiO_2 NTs; (b) side view of TiO_2 NTs; (c)-(e) top views of Ag_3PO_4-TiO_2 NTs (AT1, AT2, AT3); (f) EDS spectrum of AT2

prepared TiO_2 NTs loaded with Ag_3PO_4 nanoparticles (AT2) were also investigated by checking the element signature of EDS spectrum (Fig.2(f)). The results further confirmed that the samples were composed of Ti, O, Ag and P elements. The atomic ratios of Ti, O, Ag, and P elements were 32.05%, 66.90%, 0.65%, and 0.40%, respectively, indicating the deposition of Ag_3PO_4 on the TiO_2 nanotubes.

Fig.3 shows the XRD patterns of the TiO_2 NTs and Ag_3PO_4-TiO_2 NT heterostuctural photocatalysts. The pattern of the TiO_2 NTs (Fig.3(a)) is in good agreement with those of the Ti metal phase (JCPDS file No. 05-0682) and anatase phase of TiO_2 (JCPDS file No. 21-1272). The featured diffraction peaks at 2θ values of 25.4°, 37.8°, 48.1°, and 53.9° are attributed to the (101), (004), (200), and (105) crystallographic planes of anatase TiO_2, indicating that heat treatment is beneficial for the phase transformation from amorphous TiO_2 NTs to anatase. For the Ag_3PO_4 decorated samples (AT1, AT2, and AT3), besides the diffraction peaks of Ti substrate and anatase TiO_2, new diffraction peaks appear at 2θ values of 33.3°, 36.9°, 55.0°, and 57.3°, which correspond to (210), (211), (320), and (321) crystallographic planes of Ag_3PO_4 (JCPDS file No. 6-0505), suggesting that Ag_3PO_4 nanoparticles were successfully deposited onto the TiO_2 nanotube arrays. No diffraction peaks of other impurities were found, and the lattice phase of TiO_2 NTs did not change after Ag_3PO_4 sedimentation. With the increase of concentration of Na_2HPO_4, corresponding crystal diffraction peaks of Ag_3PO_4 gradually strengthen when the amount of generated Ag_3PO_4 nanoparticles increases.

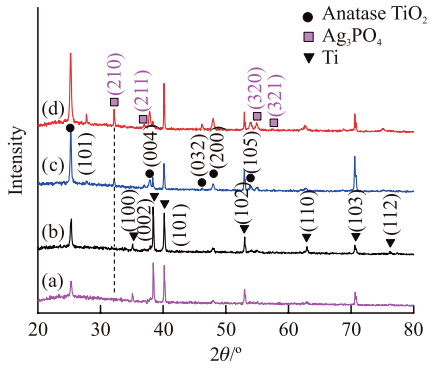

Fig.3 XRD patterns of various samples: (a) TiO_2 NTs; (b) AT1; (c) AT2; (d) AT3

UV-visible diffuse reflection spectra (DRS) were recorded to study the optical properties of samples. It can be seen from Fig.4 that TiO_2 NTs have strong absorption with a wavelength less than 390 nm, corresponding to 3.2 eV of band gap energy. Compared

with pure TiO_2 NTs, Ag_3PO_4-TiO_2 NT heterostuctural photcatalysts show the strong absorption in both ultraviolet and visible light area. In addition, AT2 has the strongest absorption in the four samples and its concentration ratio of $c(Ag_3PO_4)/c(Na_2HPO_4)$ is 1:5. This feature of UV-vis light absorption suggests that heterostuctured Ag_3PO_4-TiO_2 NT photocatalyst enhances the visible light response and improves the utilization of solar energy to a certain extend.

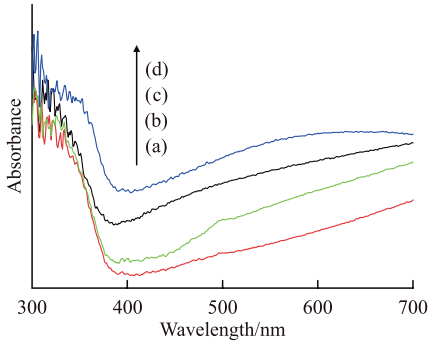

Fig.4 UV-vis diffuse reflection spectra of various samples: (a) TiO_2 NTs; (b) AT1; (c) AT3; (d) AT2

Photocurrent response can be used as a measurement of the separation efficiency of photo-generated charges. The transient photocurrent response of the TiO_2 NTs and Ag_3PO_4/TiO_2 NT photoanodes was recorded via several on-off cycles of irradiation to give further evidence for the photocatalystic activity of Ag_3PO_4/TiO_2 NTs (Fig.5). The photocurrents of the pure TiO_2 photoanode and modified photoanode in the dark are almost zero. Under simulated solar light illumination, the photocurrent density of Ag_3PO_4-TiO_2 NT is greater than 2.60 $mA{\cdot}cm^{-2}$, whereas that of TiO_2 NTs is 0.83 $mA{\cdot}cm^{-2}$, indicating that decoration of Ag_3PO_4 nanoparticles remarkably improves photocurrent density of Ag_3PO_4/TiO_2 NT heterostructure. Therefore, superior photocurrent density of Ag_3PO_4/TiO_2 NT heterostructure over that of blank TiO_2 NTs suggests a more efficient separation and longer lifetime of photo-

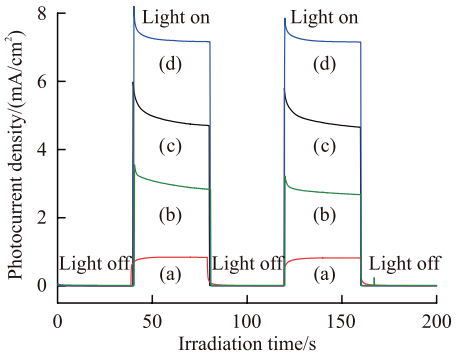

Fig.5 The photocurrent curves of various samples: (a) TiO_2 NTs; (b) AT1; (c) AT3; (d) AT2

excited electron-hole charge carriers over Ag_3PO_4/TiO_2 NT heterostructure. With increasing concentration of Na_2HPO_4, the photocurrent density further increases. When the concentration ratio of $c(AgNO_3):c(Na_2HPO_4)$ is 1:5, Ag_3PO_4/TiO_2 NT photoanode (AT2) possesses the highest photocurrent density of 7.16 $mA\ cm^{-2}$, in agreement with the results obtained by UV-visible diffuse reflection spectra.

To investigate the photocatalytic activity of the samples, photocatalytic degradation of methyl orange was tested using the simulated solar light illumination. Fig.6(a) displays the photodegradation of MO as a function of irradiation time with different photocatalysts. It can be seen from Fig.6(a) that all the Ag_3PO_4-TiO_2 NT hybrids exhibit higher photocatalytic activity than pure TiO_2 NTs. The apparent rate constants (k) calculated from the degradation curves of $-\ln(C/C_0)$ versus irradiation time are 0.00509, 0.00647, 0.00995, and 0.00648 min^{-1} for TiO_2, AT1, AT2, and AT3, respectively. These results show that AT2 possesses the highest photocatalytic rate, which is about 2 times that of pure TiO_2 NTs. The probable reason is that the Ag_3PO_4-TiO_2 NT heterostructure is constructed and an internal electric field forms to transfer photo-generated carriers and promote the separation of photo-generated electron-hole pairs. In addition, the optical response of TiO_2 NT loaded with Ag_3PO_4 extends to the visible light region, and thus improves its activity under visible light. To evaluate the stability and reusability of Ag_3PO_4-TiO_2 NT heterostructures, additional experiments of AT2 sample to degrade MO were carried out under visible light cycled for four runs. As shown in Fig.6(b), the activity of AT2 sample decreases evidently at the second run. The reason for this is that a small number of Ag_3PO_4 particles loaded on the surface of TiO_2 NTs dissolve in photocatalytic process, and at the same time part of Ag_3PO_4 nanoparticles are decomposed into silver element under illumination. With the illumination time extended, the photocatalytic performance of third and fourth runs is stable, implying a good stability of photocatalyst. Multiple loop performance of Ag_3PO_4-TiO_2 NTs is superior to that of TiO_2 NTs. The origin of its high performance of Ag_3PO_4 is that the formation of PO_4 tetrahedral units with strong P-O bonds weakens the covalent nature of the Ag-O bonds, which is advantageous for the carrier transfer to surface[20, 21]. When the concentration of $AgNO_3$ unchanges, the number of Ag_3PO_4 nanoparticles gradually increases with increasing concentration of Na_2HPO_4. When the concentration ratio of $c(AgNO_3):c(Na_2HPO_4)$

is 1:5, the photocatalytic activity is the best, which is 2 times that of undecorated TiO_2 NTs. While the concentration ratio of $c(AgNO_3)$:$c(Na_2HPO_4)$ reaches 1:10, the photocatalytic activity declines, but is still better than that of pure TiO_2 NTs. It is accepted that high concentration of Na_2HPO_4 leads to the generation of larger Ag_3PO_4 particles, which blocks TiO_2 NT channels, as shown in Fig.2(e). Therefore, the separation efficiency of photo-generated carriers decreases, thus causing lower photocatalytic performance.

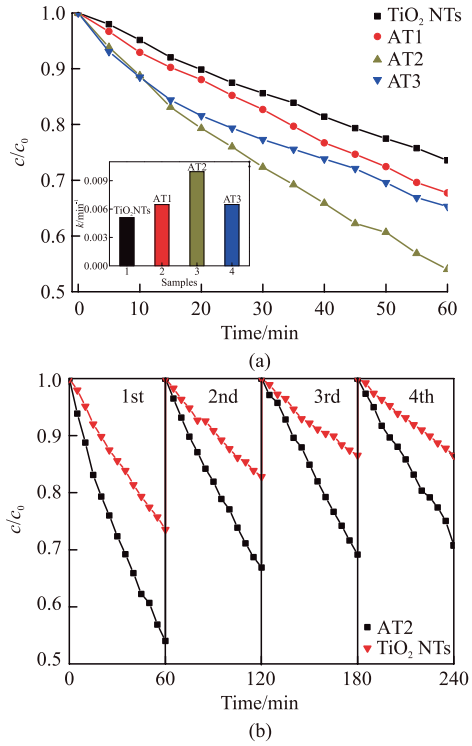

Fig.6 Photocatalytic activity of samples under the illumination with simulated solar light: (a) the rate constant of the MO decomposition by various photocatalysts: TiO_2 NTs, AT1, AT2 and AT3; (b) the compared photocatalytic performance of TiO_2 NTs and AT2 photocatalysts

Based on our previous study, a photoinduced self-stabilizing mechanism was proposed to account for the formation of stable Ag-based photocatalysts[22,23]. Namely, instable Ag_3PO_4 can be transformed into a stable Ag-Ag_3PO_4 photocatalyst after *in situ* formation of partial Ag on the surface of Ag_3PO_4 nanoparticles loaded on TiO_2 NTs. The conduction band (CB) and valence band (VB) potentials of Ag_3PO_4 are +0.4 eV and 2.9 eV versus normal hydrogen electrode (NHE), respectively[15]. In Ag_3PO_4-TiO_2 NT heterojunction, the VB edge potential of TiO_2 (+2.7 versus NHE[24]) is higher than that of Ag_3PO_4, while the CB of TiO_2 (−0.45 eV versus NHE[24]) is lower than that of Ag_3PO_4. Fig.7 shows the photocatalytic reaction mechanism for Ag_3PO_4-TiO_2 NTs under simulated solar light irradiation, indicating that the separation of electrons and holes follows two aspects: TiO_2 produces photo-generated electron-hole pairs under ultraviolet absorption, some electrons transfer from CB of TiO_2 to the surface of Ag_3PO_4, and further transfer to silver nanoparticles generated by the decomposition of Ag_3PO_4 nanoparticles. As for the photo-generated electron-hole pairs produced by Ag_3PO_4, since the VB position of Ag_3PO_4 is lower than that of TiO_2, holes migrate from the VB of Ag_3PO_4 to the VB of TiO_2. The holes trapped in the VB of TiO_2 serve as reactive species for the degradation of organic pollutants. These two paths make the separation of photo-generated electrons and holes and effectively suppress the combination of carriers, thus improving the photocatalytic activity. With increasing content of Ag_3PO_4 particles, the contact area between Ag_3PO_4 nanoparticles and TiO_2 NTs decreases. Moreover, many modified Ag_3PO_4 nanoparticles grow on the surface of TiO_2 NTs, which becomes the recombination centers of electrons and holes, and thus the photocatalystic activity of Ag_3PO_4-TiO_2 NTs declines.

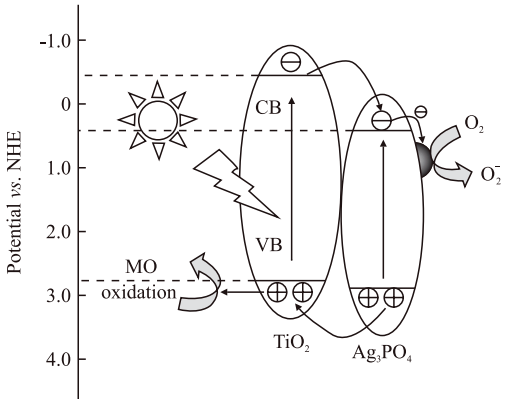

Fig.7 Schematic diagram for photocatalytic reaction of Ag_3PO_4-TiO_2 NTs under the illumination with simulated solar light

According to the above analysis, the reaction processes of photocatalytic degradation are summarized in the following equations, where, h^+ denotes the hole of the valence band, and e^- denotes the electron of the conduction band.

$$TiO_2 + h\nu \rightarrow h^+ + e^- \quad (1)$$

$$TiO_2(e^-) + Ag_3PO_4 \rightarrow TiO_2 + Ag_3PO_4(e^-) \quad (2)$$

$$Ag_3PO_4 + h\nu \rightarrow h^+ + e^- \quad (3)$$

$$Ag_3PO_4(e^-) + Ag \rightarrow Ag_3PO_4 + Ag(e^-) \quad (4)$$

$$e^- + O_2 \rightarrow O_2^- \quad (5)$$

$$h^+ + H_2O \rightarrow \cdot OH + H^+ \quad (6)$$

O_2^-, $\cdot OH$, h^+ + MO → H_2O + CO_2 + other inorganic molecules (7)

4 Conclusions

In summary, a novel Ag_3PO_4-TiO_2 NT heterostructure, in which Ag_3PO_4 nanoparticles decorated on highly ordered TiO_2 nanotube arrays, has been synthesized by a two-step anodic oxidation method and then by a deposition-precipitation method to load Ag_3PO_4. Under simulated solar light irradiation, the photocatalytic degradation rate of methyl orange with Ag_3PO_4-TiO_2 NTs is significantly higher than that with bare TiO_2 NTs. It is suggested that photo-generated electrons in TiO_2 can be quickly transferred to the conduction band of Ag_3PO_4, while photo-generated holes in Ag_3PO_4 can be transferred to the valence band of TiO_2. The photo-generated charge separation at the interface of Ag_3PO_4-TiO_2 NT heterostructure suppresses the recombination of photo-generated electron-hole pairs and leads to an enhanced photocatalytic activity and stability of Ag_3PO_4-TiO_2 NTs. In addition, the formation of Ag_3PO_4-TiO_2 NT heterostructure increases the absorption of ultraviolet and visible light and improves the utilization of solar light. The concept of constructing Ag_3PO_4-based heterostuctural photocatalyst for photo-generated charge separation can also be extended to design and develop other highly efficient photocatalysts.

References

[1] Wang P, Wang J, Ming TS, *et al*. Dye-sensitization-induced Visible-light Reduction of Graphene Oxide for the Enhanced TiO_2 Photocatalytic Performance[J]. *ACS Appl. Mater. Interface*, 2013, 5: 2924-2 929

[2] Yin SM, Yang M, Yan YW. Preparation of V-doped TiO_2 Photocatalysts by the Solution Combustion Method and Their Visible Light Photocatalysis Activities[J]. *J. Wuhan Univ. Technol.-Mater. Sci. Ed.,* 2014, 36:5 863-868

[3] Zhang QH, an X, Shao R, *et al*. Preparation of Nano-TiO_2 by Liquid Hydrolysis and Characterization of Its Antibacterial Activity[J]. *J. Wuhan Univ. Technol.-Mater. Sci. Ed*., 2014, 36: 2 407-409

[4] Albu SP, Kim D, Schmuki P. Growth of Aligned TiO_2 Bamboo-type Nanotubes and Highly Ordered Nanolace[J]. *Angew. Chem*., 2008, 120: 10 1942-1945

[5] Macák JM, Tsuchiya H, Schmuki P. High-aspect-ratio TiO_2 Nanotubes by Anodization of Titanium[J]. *Angew. Chem*., 2005, 44: 14 2100-2102

[6] Guan DS, Hymel PJ, Wang Y. Growth Mechanism and Morphology Control of Double-layer and Bamboo-type TiO_2 Nanotube Arrays by Aanodic Oxidation[J]. *Electrochimica Acta*, 2012, 83: 0 420-429

[7] Lin J, Guo M, Yip CT, *et al*. High Temperature Crystallization of Free-standing Anatase TiO_2 Nanotube Membranes for High Efficiency Dye-sensitized Solar Cells[J]. *Adv. Funct. Mater*., 2013, 23: 47 5952-5960

[8] Shrestha NK, Macak JM, Schmidt-Stein F, *et al*. Magnetically Guided Titania Nanotubes for Site-selective Photocatalysis and Drug Release[J]. *Angew. Chem*., 2009, 48: 5 969-972

[9] Liu N, Lee K, Schmuki P. Reliable Metal Deposition into TiO_2 Nanotubes for Leakage-free Interdigitated Electrode Structures and Use as a Memristive Electrode[J]. *Angew. Chem*., 2013, 52: 4 712 381-12 384

[10] Lee K, Hahn R, Altomare M, *et al*. Intrinsic Au Decoration of Growing TiO_2 Nanotubes and Formation of a High-efficiency Photocatalyst for H2 Production[J]. *Adv. Mater*., 2013, 25: 426 133-426 137

[11] Li XH, Chen GY, Yang LB, *et al*. Multifunctional Au-coated TiO_2 Nanotube Arrays as Recyclable SERS Substrates for Multifold Organic Pollutants Detection[J]. *Adv. Funct. Mater*., 2010, 20: 172 815-172 824

[12] Fujishima A, Zhang XT, Tryk DA. TiO_2 Photocatalysis and Related Surface Phenomena[J]. *Surf. Sci. Rep*., 2008, 63: 12 515-12 582

[13] Wang P, Wang J, Wang XF, *et al*. One-step Synthesis of Easy-recycling TiO_2-rGO Nanocomposite Photocatalysts with Enhanced Photocatalytic Activity[J]. *Appl. Catal. B: Environ.*, 2013, 132-133: 0 452-459

[14] Zhao ZG, Liu ZF, Miyauchi M. Nature-inspired Construction, Characterization, and Photocatalytic Properties of Single-crystalline Tungsten Oxide Octahedra[J]. *Chem. Comm*., 2010, 46: 19 3321-3323

[15] Li GL, Liang W, Xue JB, *et al*. Electrochemical Preparation and Photoelectric Properties of Cu_2O-loaded TiO_2 Nanotube Arrays [J]. *J. Wuhan Univ. Technol.-Mater. Sci. Ed.*, 2014, 36: 23-28.

[16] Yi ZG, Ye JH, Kikugawa N, *et al*. An Orthophosphate Semiconductor with Photooxidation Properties under Visible-light Iirradiation[J]. *Nat. Mater*., 2010, 9: 7 559-7 564

[17] Bi YP, Ouyang SX, Cao JY, *et al*. Facile Synthesis of Rhombic Dodecahedral Ag*X*/Ag_3PO_4 (*X* = Cl, Br, I) Heterocrystals with Enhanced Photocatalytic Properties and Stabilities[J]. P*hys. Chem. Chem. Phys*., 2011, 13: 2 110 071-2 110 075

[18] Bi YP, Hu HY, Ouyang SX, *et al*. Photocatalytic and Photoelectric Properties of Cubic Ag3PO4 Sub-microcrystals with Sharp Corners and Edges[J]. *Chem. Comm*., 2012, 48: 313 748-313 750

[19] Yu HG, Cao GQ, Chen F, *et al*. Enhanced Photocatalytic Performance of Ag_3PO_4 by Simultaneous Loading of Ag nanoparticles and Fe(III) Cocatalyst[J]. *Appl. Catal. B: Environ*., 2014, 160-161: 0 658-665

[20] Ma XG, Lu B, Li D, *et al*. Origin of Photocatalytic Activation of Silver Orthophosphate from Ffirst-principles[J]. *J. Phys. Chem. C*, 2011, 115:114 680-114 687

[21] Umezawa N, Ouyang SX, Ye JH. Theoretical Study of High Photocatalytic Performance of Ag_3PO_4[J]. *Phys. Rev. B,* 2011, 83: 3 79-83

[22] Yu HG, Liu R, Wang XF, *et al*. Enhanced Visible-light Photocatalytic Activity of Bi_2WO_6 Nanoparticles by Ag_2O Cocatalyst[J]. *Appl. Catal. B: Environ*., 2012, 111-112: 0 326-333

[23] Yu HG, Liu L, Wang XF, *et al*. The Dependence of Photocatalytic Activity and Photoinduced Self-stability of Photosensitive AgI Nanoparticles[J]. *Dalton Trans*., 2012, 41: 34 10405-10411

[24] Serpone N, Maruthamuthu P, Pic hat P, *et al*. Exploiting the Interparticle Electron Transfer Process in the Photocatalysed Oxidation of Phenol, 2-chlorophenol and Ppentachlorophenol: Chemical Evidence for Electron and Hole Transfer between Coupled Semiconductors[J]. *J. Photochem. and Photobiol. A*, 1995, 85: 3 247-3 255